Analysis on the motion characteristics of dynamic aircraft by dual-line-array TDI CCD optical camera[*]

ZHU Lin (朱琳)[1,2], **YANG Xiu-bin** (杨秀彬)[1,3]**, **XU Chao** (徐超)[1,2], **XU Ting-ting** (徐婷婷)[1,2], and **JIANG Li** (姜丽)[4]

1. Changchun Institute of Optics, Fine Mechanics and Physics, Chinese Academy of Sciences, Changchun 130033, China

2. University of Chinese Academy of Sciences, Beijing 100049, China

3. National & Local United Engineering Research Center of Small Satellite Technology, Changchun 130033, China

4. Changchun University of Science and Technology, Changchun 130033, China

A time-differential imaging method using a dual-line-array time delayed and integration (TDI) CCD optical camera is proposed in this paper, precisely measuring the motion parameters of the dynamic aircraft. Firstly, based on the spatiotemporal information of the aircraft obtained by the optical satellites, the velocity on the image plane and the twice imaging time interval are calculated. The improved scale-invariant feature transform (SIFT) algorithm that integrates the aerodynamic configuration of the aircraft is proposed to extract the region of interest. After that, the geometric centers of the aircraft images are determined with the median method, and then the velocity vector of the aircraft can be obtained by synthesizing a variety of spatial parameters and mathematical techniques. Finally, using the snapshots of the dynamic aircraft in the area of Harbin captured by the commercial satellite JL-1, the calculated results are quite close to its actual motion characteristics, which verify our method. This paper plays a guiding role in the evaluation and surveillance of dynamic aircraft.

In the field of aerospace, space-based optical time delayed and integration (TDI) camera imaging has outstanding advantages such as high precision, good controllability, and strong anti-interference ability. High-resolution remote sensing imageries enable fast recognition and measurement of moving targets, which possess high application value[1]. With the staring imaging method, the satellite adapts its attitude in real time, whose boresight always points to a specific target. This method owns the advantages of high spatial resolution, high signal-to-noise ratio, and low power consumption[2,3]. However, staring imaging suffers from the deterioration of the image quality and limited field of view. Therefore, this method cannot adapt itself to the application of surveillance of wide-distributed dynamic targets. For the conventional push-broom scanning method, the final product can only show a static image along the satellite trajectory, and the motion characteristics of the dynamic target cannot be determined.

In recent years, most of the high-resolution satellites load both panchromatic and multi-spectral sensors in order to obtain sub-meter-level colorful remote sensing images[4]. The TDI CCD of the sensors contains four kinds of spectral bands, including panchromatic band, R band, G band, and B band. The image of the target is captured at different time on the same TDI CCD, then the final image of a high-speed object will appear smear, which provides the spatial and temporal characteristic information of the object. Etaya M et al[5] took the lead to calculate the two-dimensional navigation speed of the aircraft according to the imaging time difference and the distance between the aircraft and its smear based on Qickbird satellite. However, they did not analyze the aircraft heading problem. And the combination of multi-spectral sensors and panchromatic sensors have many disadvantages, including large spatial resolution differences and short time thresholds which will lead to large errors. Greg Easson et al[6] used differential adaptive filtering to reduce the noise of images. The recognition accuracy of moving objects was improved, but the motion characteristics were not analyzed. Tao et al[7] proposed a differential imaging model, which determined the motion parameters of dynamic targets to solve the problem of the deformation of moving targets on the

remote sensing images. However, this model had some limitations to measure the velocity and direction of high-speed flight targets.

At present, the large field of view and high-resolution satellites are prevail in the remote sensing field. Most of satellites use multi-chip TDI CCD splicing to enlarge the width of the image, for example, GF-4 developed by China[8], GEO-Oculus developed in Europe[4], and En-MAP developed by the German Aerospace Centre[9,10]. There is a spatial distance L between the multi-chip TDI CCDs, which can be utilized to provide spatiotemporal information of the dynamic target. The observed target information can be obtained from the images taken at different moments[11,12]. Based on the calculation of the dynamic target with panchromatic and multi-spectral sensors, this paper proposes a time-differential imaging method to calculate speed parameters of the dynamic target on the same band of dual-line-array TDI CCD.

Static images can be obtained with the single-line-array TDI camera. The single-line-array TDI CCD with panchromatic and multi-spectral sensors suffers from inconsistent spatial resolution of the spectral bands, and it leads to a short distance of each spectral band, which is important to capture the dynamic target at different time, especially in the case of dual-line-array TDI CCD. As shown in Fig.1, the velocity vector of the aircraft is determined by the displacement vector on the image surface and the imaging time interval.

The imaging time interval of the dynamic aircraft is the ratio of the dual-line-array TDI CCD spatial distance to the image motion velocity vector.

As shown in Fig.2, the spatial distance L between CCD1 and CCD2 of the dual-line-array TDI CCD is constant on the focal plane, because the configuration of the optical camera has been fixed since it is manufac-

tured.

As shown in Fig.1, the satellite adjusts its attitude to scan the specified ground area. The image motion velocity vector is determined in two steps. Firstly, the ground velocity vector is calculated with the earth rotation velocity and the satellite velocity relative to the earth. Secondly, the ground velocity vector is projected onto the image plane to calculate the image motion velocity vector.

The geometric relationship between the ground imaging area and the satellite position is shown in Fig.3 during the process of the satellite lateral swing imaging. The earth is approximated as a sphere in the following. O denotes the central point of the earth, and S is the position of the satellite at a certain time t. Connect SO and intersect the surface of the earth at the sub-satellite point G. The ground trajectory of the satellite orbit is CG, which locates on the orbital plane COG. GB is perpendicular to COG at point B. OB intersects the equator at point A. The surface BOG is the side view of the satellite at time t. In addition, GD is perpendicular to the equator plane AOC at point D. $\angle GSR=\varphi_0$ is the roll angle of the satellite with the boresight pointing to the earth at point R. R denotes the point with the latitude and longitude coordinate of (α_R, λ_R), which can be calculated by great-circle paths method in the spherical case. In this case, $\angle GOD=\theta$, and $\angle GCA=i_0$ denotes the orbital inclination angle. Besides that, there are some other parameters, including the earth radius r and the orbit height h. The formulas are as follows:

$$\alpha_R = \alpha - \left(\arccos\left(\frac{\cos\angle GOA}{\cos\theta} \right) - \arccos\left(\frac{\cos\angle ROA}{\cos\lambda_R} \right) \right), \quad (1)$$

$$\lambda_R = \arcsin\left\{ \frac{\sin\left\{ \arcsin\sqrt{\sin^2\theta / \left(1 - \sin^2 i_0 + \sin^2\theta\right)} - \arcsin\left[\left(1 + h/r\right)\cdot\sin\varphi_0\right] + \varphi_0 \right\}}{\sqrt{1/\left(1 - \sin^2 i_0 + \sin^2\theta\right)}} \right\}. \quad (2)$$

Fig.1 Diagram of the aircraft captured by dual-line-array TDI CCD optical camera
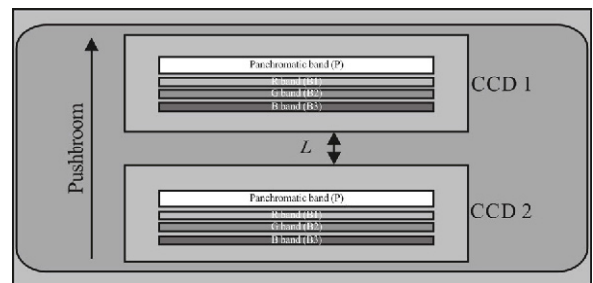

Fig.2 Structural diagram of dual-line-array TDI CCD

As shown in Fig.3, the object distance LL is between the optical center of satellite camera lens and the ground point. It is calculated as:

$$LL = (r + h) \times \cos(\varphi_i) - \sqrt{r^2 - (r+h)^2 \times \sin^2(\varphi_i)}, \quad (3)$$

where

$$\varphi_i = \varphi_0 + \eta_i, \tag{4}$$

η_i is the field of view angle of the camera. The motion velocity on the ground imaging area consists of two components. The first one is the velocity V_{es} along the direction of the push-broom caused by the satellite orbital motion:

$$V_{es} = \Omega \cdot [(r+h) - \cos\varphi_i \cdot LL], \tag{5}$$

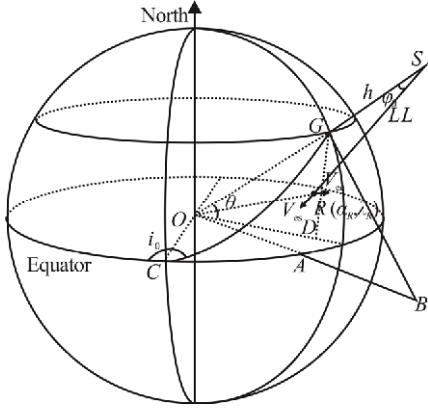where Ω is the orbital angular velocity.

Fig.3 Geometric relationship diagram of satellite side pendulum imaging

The other is the tangential velocity V_{ee} on the ground scene caused by the Earth's spinning motion:

$$V_{ee} = \omega \cdot r \cdot \cos\lambda_R, \tag{6}$$

where ω is the angular velocity of earth rotation, and λ_R is the latitude of the object point on the ground.

The velocity vector of R is projected from the ground coordinate system into the image coordinate system to calculate the image motion velocity vector.

The velocity vector V in the object coordinate system is calculated as

$$V = \begin{bmatrix} V_1 \\ V_2 \\ V_3 \end{bmatrix} = \begin{bmatrix} V_{es} - V_{ee}\cos i_0 \\ V_{ee}\sin i_0 \\ V_{ee}\sin i_0 \cos\varphi_i \end{bmatrix}, \tag{7}$$

where V_1 and V_2 are the longitudinal and lateral velocity of the target along the sub-satellite trajectory respectively, and V_3 is the velocity along the optical axis.

By transforming coordinate systems, the image motion velocity vector V_p of the point on the overlapping area is expressed as:

$$V_p =$$

$$\begin{bmatrix} V_{p1} \\ V_{p2} \\ V_{p3} \\ 0 \end{bmatrix} = \begin{bmatrix} -\dfrac{f}{LL} & 0 & 1 & 0 \\ 0 & -\dfrac{f}{LL} & 1 & 0 \\ 0 & 0 & 0 & 0 \\ 0 & 0 & 0 & 0 \end{bmatrix} \begin{bmatrix} V_1 \\ V_2 \\ V_3 \\ 1 \end{bmatrix} = \begin{bmatrix} -\dfrac{f}{LL}V_1 \\ -\dfrac{f}{LL}V_2 \\ 0 \\ 0 \end{bmatrix}. \tag{8}$$

It is clear that V_p is irrelevant with V_3, and it is expressed as

$$V_p = \sqrt{V_{p1}^2 + V_{p1}^2}. \tag{9}$$

The drift angle is between the push-broom direction of the TDI camera and the sub-satellite trajectory, and it is expressed as:

$$\beta = \arctan(V_{p2}/V_{p1}). \tag{10}$$

The imaging time interval of the sub-satellite point is calculated as:

$$T = \frac{L}{V_p}, \tag{11}$$

where L is the distance between the interleaved TDI CCD.

CCD1 captures the image of the target before CCD2 due to the existence of the distance L between two CCDs. The same dynamic target occurs twice in the registered image. The displacement vector of the target depends on the distance of the geometric center points of the dynamic targets and the time interval T. In order to achieve information of the aircraft on the image plane, high-precision extraction of the feature points in the image is required. The pipelines are as follows: firstly, use the improved SIFT algorithm to obtain the region of interest (ROI) in order to extract and mark the targets; secondly, binarize the images and reduce the noise; finally, use the image median method to determine the centers of the targets.

This paper proposes an improved scale-invariant feature transform (SIFT) algorithm based on the aerodynamic configuration of the aircraft. The algorithm can eliminate the non-aircraft targets in the image and shorten the run time of the SIFT algorithm. Firstly, the aerodynamic configuration of the general aircraft is used to eliminate the non-aircraft targets from the image. The aerodynamic configuration characteristics of aircraft have the following features:
1) Symmetry: the axisymmetric degree of the aircraft (1 ± 0.3);
2) Aspect ratio: the ratio of length to diameter of the aircraft fuselage (7.279 1—20.263 2);
3) Ratio of wing's trapezoid: the ratio of the projection of the airfoil to that of its largest external right-angled trapezoid (0.608 9—0.916 4);
4) Ratio of fuselage's area: the ratio of the fuselage area to the overall area of the aircraft (0.223 9—0.525 8);
5) Ratio of trapezoid's leading edge: the ratio of the distance between the leading edge of the airfoil and the nose to the length of the entire fuselage (0.156 7—0.439 8).

As shown in Fig.4(a)—(e), the five features mentioned above show their own constraints for different types of aircraft. The flight altitude of the aircraft is 5—20 km and orbital height of the satellite is 300—1 000 km. The photographing angle has little effect on the snapshots of the aerodynamic configuration of the aircraft due to the large height difference between the satellite and the aircraft. Using a sample library with a certain number of samples, aircraft targets can be well distinguished.

The SIFT algorithm is further used to identify the aircraft image based on enough features matched, then the ROI can be obtained.

As shown in Fig.5(a), the aircraft is selected as the target to be matched; the other aircraft is shown in

Fig.5(b) as a reference, and there are some other types of aircraft included in the sample library. Firstly, the aerodynamic structural characteristics of Fig.5(a) is calculated in this case. The aspect ratio is 11.149 2, the ratio of trapezoid's leading edge is 0.371 8, and the symmetry is 0.750 8, which basically satisfy the characteristics of the aircraft. Then the target image is compared with the images in the sample library, and the evaluation criteria for a successful recognition is the number of matched feature points. Fig.5(c) and Fig.5(d) show the results, which have one and 9 matching points, respectively. It can be seen in Fig.5(d) that the object to be identified in the Fig.5(a) matches the aircraft in the Fig.5(b) in the sample library. When the sample size is large enough and the number of matching points is sufficient, if the model of the standard aircraft in the library is already known, the target model can be further inferred.
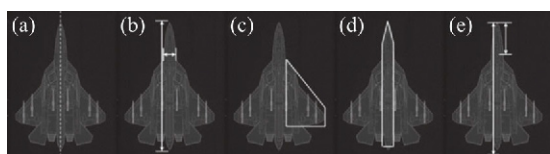

Fig.4 Characteristics of aerodynamic configuration: (a) Symmetry; (b) Aspect ratio; (c) Ratio of wing's trapezoid; (d) Ratio of fuselage's area; (e) Ratio of trapezoid's leading edge
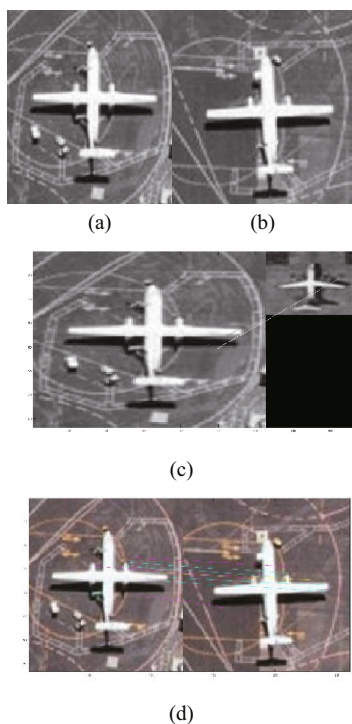

Fig.5 SIFT matching integrated with aircraft aerodynamic configuration features: (a) The passenger aircraft to be matched; (b) A standard passenger airport in the sample library; (c) A failed matching with one feature point; (d) A successful matching with 9 feature points

The optimal threshold of the original picture is determined by the method of maximum classes square error. The pixel values of the target object and the background are 1 and 0, respectively. Then, the image opening operation is used to remove the noise and obtain the binary image as shown in Fig.6.
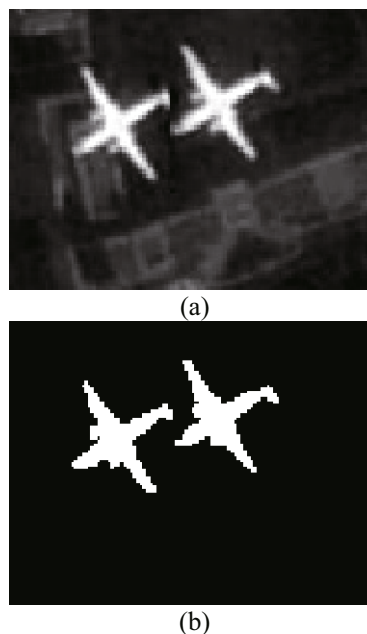

(a)

(b)

Fig.6 Binary processing diagrams of the target aircraft: (a) Original area map of the target aircraft; (b) Binary map of the target aircraft

The dual-line-array TDI CCD camera snapshots the same high-speed aircraft at different time. The aircraft images will be blurred after magnified due to the limitation of spatial resolution. If the displacement is calculated using the feature points, the error will be quite large. Therefore, in this section the center of the overall aircraft image is utilized, and the image median method is used to calibrate the center of the aircraft. The equations are listed as follows:

$$Q(x) = \sum_{x_{\min}}^{x} \sum I(x, y), \tag{12}$$

$$Q(x_i) = \frac{1}{2}\left[Q(x)_{\max} - Q(x)_{\min}\right], \tag{13}$$

$$Q(y) = \sum_{y_{\min}}^{y} \sum I(x, y), \tag{14}$$

$$Q(y_i) = \frac{1}{2}\left[Q(y)_{\max} - Q(y)_{\min}\right], \tag{15}$$

where Q is the area occupied by the aircraft, I is the gray value of point (x, y), and (x_i, y_i) is the center of the target on the graph.

As shown in Fig.7, the snapshots of the same scene at two different moments appear on the image surface after stitched, when camera captures the high-speed moving aircraft. The centers of two profiles on the image surface

are determined by the median method, and their coordinates are expressed as (x_1, y_1) and (x_2, y_2), respectively. a is the pixel size. Finally, the number of pixels between the two centers is obtained,

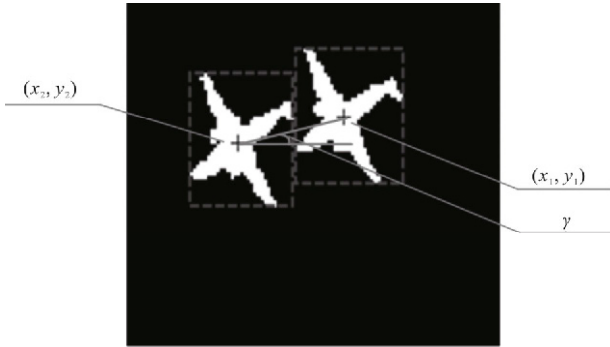$$n = \frac{\sqrt{(x_2^2 - x_1^2) + (y_2^2 - y_1^2)}}{a}. \tag{16}$$

Fig.7 Center extraction map of the moving target

The angle γ is between the sub-satellite trajectory and the aircraft navigation direction,

$$\gamma = \arctan[(y_1 - y_2)/(x_1 - x_2)]. \tag{17}$$

The velocity and the flight direction of the dynamic aircraft are of great importance to measure the motion characteristics. The flight direction is based on the geographical position, and it is first calculated on the image plane. Synthesized with orbital parameters, image motion vectors and the velocity vector of dynamic target, an equation of aircraft flight direction is established in the section.

The velocity of the dynamic aircraft is determined by the imaging time interval and the distance between the aircraft and its smear on the focal plane. The velocity can be expressed as

$$v = \frac{na \times LL}{T \times f}. \tag{18}$$

Schematic diagram of aircraft navigation direction is shown in Fig.8. i_0 denotes the orbital inclination, and the drift angle β is between the push-broom direction and the sub-satellite trajectory. The angle between the aircraft navigation direction and geographical north is δ. Therefore, the actual course of the aircraft δ

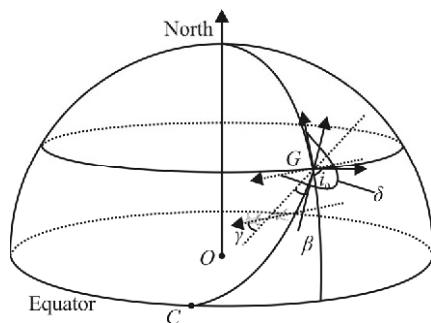$$\delta = i_0 + \beta + \gamma + 90°. \tag{19}$$

Fig.8 Schematic diagram of plane navigation direction

On-orbit simulation experiments using the commercial satellite JL-1 have been conducted to verify our proposed method. The interlace-stitched TDI CCD on the JL-1 is an equivalent of the dual-line-array TDI CCD in this paper, and it captured the dynamic aircraft in the urban area of Harbin. With the satellite push-broom scanning along the orbit, it gets two snapshots of the aircraft at the staggered lap. After precisely registered, two identical aircraft profiles will appear in the same image. The imaging process and the image are shown in Fig.9(a) and (b), respectively.
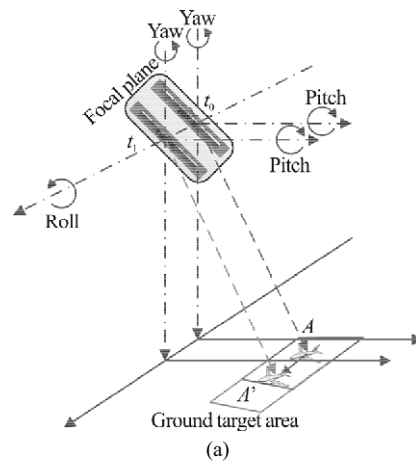

(a)

(b)

Fig.9 Schematic diagrams of aircraft imaging using JL-1: (a) On-orbit experiment of JL-1 satellite; (b) JL-1 satellite imaging

The related imaging parameters are shown in Tab.1.

Tab.1 Imaging parameters on orbit

Original parameter	Value
Two TDI CCDs' spacing	23 mm
Pixel size	8.75 μm
Radius of the earth	6 370.04 km
Orbit height	656 km
Roll angle	2.9°
Orbital inclination	98.02°
Latitude of sub-satellite point	46.22°
Longitude of sub-satellite point	126.74°
Camera focal length	8 m

When the roll angle of the satellite is 2.9°, the field of view angle is very small, then the object distance can be calculated according to Eq.(3),

$$LL=656.828\ 0\ \text{km}. \tag{20}$$

The image motion velocity can be confirmed as

$$V_P = \sqrt{V_{p1}^2 + V_{p2}^2} = 84.072\ 9\ \text{mm/s}. \tag{21}$$

The drift angle can be obtained,

$$\beta = \arctan(V_{p2}/V_{p1}) = 3.825\ 9°. \tag{22}$$

The twice imaging interval of dual-line-array TDI CCD camera can be expressed as

$$T = \frac{L}{V_p} = 0.273\ 6\ \text{s}. \tag{23}$$

After processing the on-orbit images, the difference in number of pixels between two centers can be calculated as $\Delta x=32$, $\Delta y=6$, $n=32.557\ 6$. The angle between the aircraft navigation direction and the satellite moving direction can be determined as $\gamma=10.619\ 7°$.

The velocity of the aircraft is determined by the imaging time interval and the distance between the aircraft and its smear on the focal plane, and it is calculated as

$$v = \frac{na \times LL}{T \times f} = 85.509\ 9\ \text{m/s} = 307.835\ 7\ \text{km/h}. \tag{24}$$

The angle between the flight direction of the aircraft and the north of the image plane can be calculated as

$$\delta = 98.020\ 0° + 3.825\ 9° + 10.619\ 7° +$$
$$90.000\ 0° = 202.465\ 5°. \tag{25}$$

According to the calculated results, the velocity of the aircraft is 307.835 7 km/h, and the course is 202.465 5°. It can be speculated from the aircraft's geographical position that the aircraft is slowing down and flying to Harbin Taiping International Airport.

Two kinds of error should be considered when calculating the velocity of a dynamic target, including distance error and time error. The former one mainly results from the position error when the satellite scans the target, and the position error of extracted image center is usually less than ±1 pixel. The error of the TDI CCD imaging time interval is determined by two TDI CCD spacing and image motion speed. The calibration accuracy of the spacing of the dual-line-array TDI CCD is less than 1 μm, and the calibration accuracy of the image motion speed is 0.05%. Therefore, the error of TDI CCD imaging time interval is 0.05—0.1 ms. Synthesized with all the errors mentioned above, the speed error range of the aircraft is 298.201—317.471 km/h, and the maximum error rate is 3.13%. The inaccuracy of the aircraft direction is mainly affected by three factors, including the orbital inclination, the drift angle and the angle γ. Wherein, the on-orbit GPS tilt error is less than 0.01°, and the drift angle error is less than 0.05°. The error of γ is less than 0.15°. In conclusion, the actual navigation direction error of the aircraft is 0.21°.

This paper proposes an innovate method the velocity of the dynamic flight aircraft. The method is verified by using JL-1, and all the parameters of the experiment including the spatial distance L between two TDI CCDs, imaging time interval, and the image motion velocity vector and the orbital elements are calibrated on orbit. The flight state and the direction of the aircraft can be accurately predicted. We can safely draw a conclusion that the calculation results are effective and the calculation accuracy can be ensured.

Our method is more accurate and reliable compared with the conventional methods in the relevant field, and it is believed that the method proposed in this paper will play a guiding role and have some certain application value in the field of dynamic aircraft monitoring, military air defense, and so on.

References

[1]   Xu Wei, Chen Yan-tong, Piao Yong-jie and Wang Shao-ju, Optics & Precision Engineering **25**, 255 (2017). (in Chinese)

[2]   Yang Xu-bin, Jiang Li, Wang Shao-ju, Wang Min, Fan Guo-wei and Wang Ya-min, Acta Optica Sinica **37**, 123 (2017). (in Chinese)

[3]   Huang Fu-yu, Shen Xue-ju, Liu Xu-min and Cui Tie-cheng, Optics & Precision Engineering **23**, 2328 (2015). (in Chinese)

[4]   Vaillon L., Schull U., Knigge T. and Bevillon C., SPIE **0277**, 786X (2017).

[5]   Etaya M., Sakata T., Shimoda H. and Mastumae T., Journal of the Remote Sensing Society of Japan **24**, 357 (2003).

[6]   Easson G., Delozier S. and Momm H G., Remote Sensing **2**, 1331 (2010).

[7]   Tao Jiang-wei, Research on Methods and Techniques for Obtaining Motion Parameters of Objects in High-resolution Satellite Images, Peking University, 2009. (in Chinese)

[8]   Ma Wen-po and Li Min-long, Spacecraft Recovery & Remote Sensing **37**, 26 (2016).

[9]   Heiden U., Mueller A., Guanter L. and Storch T., Geoscience, Remote Sensing Symposium. IEEE, 439 (2017).

[10]   Guanter L., Kaufmann H., Segl K., Foerster S., Rogass C., Chabrillat S., Kuester T., Hollstein A., Rossner G., Chlebek C., Straif C., Fischer S., Schrader S., Storch T., Heiden U., Mueller A., Bachmann M., Mühle H., Müller R., Habermeyer M., Ohndorf A., Hill J., Buddenbaum H., Hostert P., Van der Linden S., Leitão P.J., Rabe A., Doerffer R., Krasemann H., Xi H., Mauser W., Hank T., Locherer M., Rast M., Staenz K. and Sang B., Remote Sensing **7**, 8830 (2015).

[11]   Jiang Li, Yang Xiu-bin, Wang Ya-min and Su Chang, Laser & Optoelectronics Progress **53**, 177 (2016). (in Chinese)

[12]   Xu Wei, Jin Guang and Wang Jiaqi, Optics & Precision Engineering **25**, 1969 (2017). (in Chinese)